Classifying regimes of atmospheric circulation in terms of their global super-rotation

Neil T. Lewis*, Greg J. Colyer and Peter L. Read

Atmospheric, Oceanic and Planetary Physics
Department of Physics, Clarendon Laboratory, University of Oxford, UK

ABSTRACT

The global super-rotation index S compares the integrated axial angular momentum of the atmosphere with that of a state of solid-body co-rotation with the underlying planet. S is similar to a zonal Rossby number, which suggests its value may be a useful indicator of the circulation regime occupied by a planetary atmosphere. In this work, we investigate the dependence of S on planetary rotation rate, Ω, by running idealised Earth-like general circulation model experiments over a wide range of rotation rates, in both an axisymmetric and three-dimensional configuration. Across the range of rotation rates considered – $8\Omega_{\mathrm{E}}$ to $\Omega_{\mathrm{E}}/512$, where Ω_{E} is the Earth's rotation rate – S is of the same order of magnitude in the 3D and axisymmetric experiments. For high rotation rates, we find that $S \ll 1$ and $S \propto \Omega^{-2}$, while at low rotation rates $S \approx 1/2 = \text{constant}$. By considering the limiting behaviour of theoretical models for S, we show that the value of S and its local dependence on Ω can be used to define the circulation regime occupied by a planetary atmosphere. $S \ll 1$ and $S \propto \Omega^{-2}$ defines a circulation regime dominated by geostrophic thermal wind balance, and $S \approx 1/2 = \text{constant}$ defines a regime where the dynamics are characterised by conservation of angular momentum within a planetary-scale Hadley circulation. $S \gg 1$ and $S \propto \Omega^{-1}$ defines an additional regime dominated by cyclostrophic balance and strong equatorial super-rotation. This regime, characteristic of Venus and Titan, is not realised in our numerical experiments.

1. Introduction

The dynamics of planetary atmospheres are sensitive to planetary parameters such as their radius a and sidereal rotation rate Ω, as well as atmospheric properties such as atmospheric composition. This is borne out by the dynamics of the Solar System atmospheres. The Earth's atmospheric circulation is characterised by overturning (Hadley) cells which feature air rising near the equator and sinking in the sub-tropics. In the mid-latitudes, prograde jets with zonal velocities of approximately 30–40 $\mathrm{m\,s^{-1}}$ are present, while in the tropics weak retrograde flow is found (Schneider 2006). By contrast, Venus and Titan (which are slowly rotating with respect to the Earth, and in the case of Titan also smaller) host prograde equatorial jets with zonal wind velocities in excess of 100 $\mathrm{m\,s^{-1}}$ (Counselman et al. 1980; Bird et al. 2005). Numerical modelling suggests these atmospheres also feature planetary-scale overturning circulations formed of Hadley-like cells with a nearly hemispheric meridional extent (Hourdin et al. 1995; Lebonnois et al. 2010). The atmospheres of the gas giant planets Jupiter and Saturn (much larger and more rapidly rotating with respect to the Earth) feature zonal velocity profiles with strongly prograde jets alternating with weakly retrograde jets in a banded pattern (Porco et al. 2003, 2005).

There is now a large body of work that seeks to understand how atmospheric circulation is sensitive to key parameters and processes [as detailed in reviews by Read (2011), Showman et al. (2013), and Read et al. (2018)]. Numerical modelling using Earth-like General Circulation Models (GCMs; Earth-like as they have a radiative heating/cooling structure that mimics the Earth's, and use Earth's surface pressure) has revealed that the external thermal Rossby number

$$\mathcal{R} \equiv \frac{R_{\mathrm{d}}\Delta T_{\mathrm{eq}}}{(\Omega a)^2}, \tag{1}$$

is an important parameter in determining the dynamical regime occupied by a planetary atmosphere (Geisler et al. 1983; Williams 2003; Mitchell and Vallis 2010; Potter et al. 2014; Kaspi and Showman 2015; Wang et al. 2018). Above, R_{d} is the specific gas constant for dry air (where 'air' is the main atmospheric constituent), and ΔT_{eq} is the radiative equilibrium equator-to-pole temperature contrast.

The numerical experiments presented in the studies listed above show that for $\mathcal{R} \ll 1$ (rapid rotation rate), a regime characterised by geostrophic balance and multiple zonal jets is obtained. For $\mathcal{R} \gg 1$ (slow rotation rate), atmospheric circulations typically occupy a regime characterised by cyclostrophic balance and a super-rotating equatorial jet, with specific zonal angular momentum greater than that of the underlying planet at the equator. The emergence of strong super-rotation in simulations with large $\mathcal{R}$ is consistent with the existence of super-rotation in the atmospheres of Venus and Titan, for which $\mathcal{R}_{\mathrm{V}} \approx 570$ and $\mathcal{R}_{\mathrm{T}} \approx 20$ respectively (Read and Lebonnois 2018).

*Corresponding author: Neil T. Lewis, neil.lewis@physics.ox.ac.uk

A planet's atmospheric circulation is not solely determined by $\mathcal{R}$ however, as it is sensitive to other non-dimensional parameters [such as the Ekman number or frictional Taylor number, and the thermal damping number; Potter et al. (2014); Dias Pinto and Mitchell (2014); Wang et al. (2018)]. For example, Dias Pinto and Mitchell (2014) show that when $\mathcal{R}$ is large, a strongly super-rotating state – analogous to that of Venus' and Titan's atmospheres – is not obtained if the thermal damping number $\hat{\tau}_{\mathrm{a}} = 2\Omega\tau_{\mathrm{a}}$, where τ_{a} is a radiative relaxation timescale, is small (as may be typical for a slowly rotating planet). This underscores the importance of other differences between Venus and Titan, and Earth-like planets, beyond Venus' and Titan's large external Rossby numbers, for generating strong super-rotation.

To facilitate the comparison of circulation regimes obtained in different planetary atmospheres, it is useful to develop bulk quantities that indicate the specific regime they occupy. However, the utility of $\mathcal{R}$ and other input parameters for this task is limited, by the sensitivity of atmospheric circulation to multiple input parameters and atmospheric properties. Instead, it is necessary to use diagnostic quantities that can be computed from the equilibrium flow structure in a planetary atmosphere (or a set of numerical simulations).

In this study, we will investigate the utility of the global super-rotation index S for characterising and comparing the circulation regimes occupied by different planetary atmospheres. S is defined (Read 1986a,b; Read and Lebonnois 2018)

$$S \equiv \frac{\int \rho m \,\mathrm{d}V}{\int \rho \Omega a^2 \cos^2\vartheta \,\mathrm{d}V} - 1, \tag{2}$$

and compares the mass-weighted global integral of the specific zonal angular momentum

$$m = a\cos\vartheta(\Omega a \cos\vartheta + u), \tag{3}$$

with a state of solid-body co-rotation with the underlying planet (when $S > 0$ the atmosphere has more zonal angular momentum that if it were co-rotating with the planetary surface). Above, $\mathrm{d}V = a^2\cos\vartheta\,\mathrm{d}\lambda\,\mathrm{d}\vartheta\,\mathrm{d}z$ is an element of volume, ϑ, λ, and z are the latitude, longitude, and height coordinates, respectively, u is the zonal wind velocity, and ρ is the density.

S can be regarded as the quotient of a mean zonal velocity U, and Ωa, and thus shares some characteristics of a zonal Rossby number [see, e.g., Read (1986a)]. This suggests that S may be a useful quantity to compute when comparing planetary atmospheres, as its value is *indicative* of the dynamical regime occupied by an atmosphere. $S \ll 1$ is suggestive of a regime where the dynamics are dominated by geostrophic balance, and $S \gg 1$ suggests a regime where the dynamics are dominated by cyclostrophic balance. S is given further value by the fact that it is constrained to be $S \leq 1/2$ in an axisymmetric, inviscid atmosphere. The constraint is due to Hide's theorem (Hide 1969), which states that in an axisymmetric, inviscid setting, $\mathrm{D}m/\mathrm{D}t = 0$. If we assume that in a thin boundary layer, surface friction acts to restore m to a state of co-rotation with the underlying planet, then the maximum value of m that may be obtained in the boundary layer is $m = \Omega a^2$ (the value of m for a parcel of air co-rotating with the planetary surface at the equator). Parcels of air that are then transported into the free atmosphere (e.g., by an overturning circulation) will then also have $m \leq \Omega a^2$, as m is materially conserved. The $S = 1/2$ limit corresponds to the scenario where $m = \Omega a^2$ everywhere (and the boundary layer has infinitesimal depth), and if $S > 1/2$ then non-axisymmetric disturbances which transport m up its local gradient must be present in the atmosphere.

The global super-rotation index has been used previously to compare the dynamics of the Solar System atmospheres (Read and Lebonnois 2018), and to compare different Venus and Titan GCMs (Lebonnois et al. 2012, 2013). In addition, the value of S estimated from zonal velocity measurements in Venus' atmosphere has been compared with S computed from the output of Venus GCMs to assess how well they reproduce the observed circulation (Mendonça and Read 2016; Read and Lebonnois 2018). The atmospheres of Venus and Titan, for which $S_{\mathrm{V}} \approx 7.7$ and $S_{\mathrm{T}} \approx 2$ (Read and Lebonnois 2018), exhibit the greatest degree of global super-rotation within the Solar System, and $S \gg 1$ is indicative of the dominance of cyclostrophic balance in the local momentum budget throughout the atmosphere. For Mars and the Earth, $S_{\mathrm{M}} \approx 0.04$ and $S_{\mathrm{E}} \approx 0.0135$ (Read and Lebonnois 2018), which is consistent with the dominance of geostrophic balance in the their atmospheres. The fact that $S > 1/2$ for Venus and Titan means that eddy processes, which transport m up its local gradient, *must* be important in determining the dominant (cyclostrophic) dynamical balance that characterises their atmospheric circulations.

It is of interest to understand how different atmospheric processes contribute to the value of S, and how S varies between planetary atmospheres as different parameters are varied. To date, these questions have only been investigated using axisymmetric models with an eddy-viscosity parametrisation that diffuses angular velocity, which allows for up-gradient transport of m (Read 1986a; Yamamoto et al. 2009; Yamamoto and Yoden 2013). These studies have shown that S scales with Ω^{-2} ($S \propto \mathcal{R}$) at high rotation rate (small $\mathcal{R}$), and that at low rotation rate (large $\mathcal{R}$) S either saturates (S = constant) when parametrised up-gradient transport of m is small, or scales with Ω^{-1} or $\Omega^{-2/3}$ ($S \propto \sqrt{\mathcal{R}}$ or $S \propto \mathcal{R}^{1/3}$) when the eddy diffusion coefficient is made large and up-gradient transport of m is significant. Yamamoto and Yoden (2013) develop a theory that relates S to $\mathcal{R}$, valid for slowly rotating planets with significant up-gradient transport of m. By considering the limiting behaviour of their theory, they are able to explicitly demonstrate that $S \propto \sqrt{\mathcal{R}}$ or $S \propto \mathcal{R}^{1/3}$ is associated with the dominance of cyclostrophic balance in the zonal momentum budget throughout the atmosphere.

a. Outline of paper

In this work, we investigate the dependence of S on Ω using an idealised three-dimensional (3D) Earth-like GCM [similar to those used by Geisler et al. (1983); Williams (2003); Mitchell and Vallis (2010); Potter et al. (2014); Kaspi and Showman (2015); Wang et al. (2018)]. Our aim is to identify possible scaling regimes for S in terms of Ω for the case of an Earth-like atmosphere, and the processes that determine the dependence of S on Ω.

Experiments of this type are an obvious extension to the work of Read (1986a), Yamamoto et al. (2009), and Yamamoto and Yoden (2013). Unlike in these previous studies, up-gradient transport of m in our model is not parametrised, and the existence, direction and strength of materially non-conservative transport of m is associated with the existence and characteristics of non-axisymmetric disturbances that can induce stresses on the zonal flow. To elucidate the role of eddies in determining the dependence of S on Ω, we run a set of axisymmetric (2D) experiments alongside our 3D experiments.

For both our 3D and 2D experiments, we will show that S scales with Ω^{-2} ($S \propto \mathcal{R}$) for rapid rotation rates, while for low rotation rates (large $\mathcal{R}$) $S =$ constant. To interpret these scalings for S, we derive a theory for S in terms of $\mathcal{R}$ from the axisymmetric model of Held and Hou (1980), that captures the scaling behaviour of S in our numerical experiments. As in Yamamoto and Yoden (2013), we consider the limiting behaviour of our theory to show how different dependencies of S on $\mathcal{R}$ correspond to different dominant dynamical balances.

We argue that by taking the theory we develop in this work in tandem with that of Yamamoto and Yoden (2013), the combination of the value of S and the local dependence of S on $\mathcal{R}$ can be used to identify and compare the circulation regimes of different planetary atmospheres.

The rest of this work is structured as follows. Our model configuration and experiment design is described in Section 2. To provide context for the rest of the paper, we describe the zonally-averaged circulation obtained in our experiments in Section 3. In Section 4, we compute S for each experiment, discuss its dependence on Ω, and investigate differences in S between 3D and axisymmetric experiments. This section also includes the derivation of our theory for S for the case of an axisymmetric atmosphere in the inviscid limit. Discussion focussed on illustrating the relationship between S and circulation regime is provided in Section 5. In Section 6 we summarise our findings.

2. Experiment design

a. Numerical model

We make use of `Isca`, a framework for building idealised general circulation models of varying complexity (Vallis et al. 2018). `Isca` is built on-top of the GFDL (Geophysical Fluid Dynamics Laboratory, Princeton) primitive equation spectral dynamical core. In the present work, `Isca` is configured as a dry-dynamical core forced by Newtonian cooling to a statically stable axisymmetric radiative-convective equilibrium temperature profile.

Dynamical core

The dynamical core integrates the primitive equations forwards in time, using a semi-implicit leap-frog scheme with a Robert-Asselin time filter. The equations are solved on a thin spherical shell using a pseudo-spectral method in the horizontal (prognostic fields are represented by a triangular truncation of spherical harmonics), and a finite difference method in the vertical. For numerical efficiency, and to avoid formulation of vector fields on the spectral grid, the primitive equations are solved in terms of the scalar vorticity and divergence. The vertical coordinate is a terrain-following coordinate, defined as $\sigma_\ell = p/p_s$. There are $N = 80$ vertical levels, roughly evenly spaced in the troposphere with enhanced resolution in the stratosphere. The level boundaries are defined $\sigma_{\ell-1/2} = \exp(-\xi_{\ell-1/2} N_{\rm H})$ with $\xi_{\ell-1/2} = r_{\rm s}\ell_{\rm n} + (1-r_{\rm s})\ell_{\rm n}^{\kappa}$, where $\ell_{\rm n} = 1-(\ell-1)/N$, $r_{\rm s} = 0.5$, $\kappa = 7.5$, and $N_{\rm H} = 6$ is the number of scale heights. $\sigma_{N+1/2} = 1.0$.

Thermal forcing

The relaxation temperature profile used for the Newtonian cooling is that described in Wang et al. (2018), similar to that of Held and Suarez (1994), and is written

$$T^* = T_z^*(z) + T_\vartheta^*(\vartheta, \sigma), \tag{4}$$

where

$$T_z^* = T_z^*|_{\rm tp} + \sqrt{\left[\frac{L}{2}\left(z_{\rm tp} - z\right)\right]^2 + K^2} + \frac{L}{2}\left(z_{\rm tp} - z\right), \tag{5}$$

and

$$T_\vartheta^* = h(\sigma)\Delta T_h^* \left(\frac{1}{3} - \sin^2\vartheta\right), \tag{6}$$

with

$$h = \begin{cases} \sin\left[\frac{\pi}{2}\left(\frac{\sigma - \sigma_{\rm tp}}{1-\sigma_{\rm tp}}\right)\right], & \text{if } \sigma \geq \sigma_{\rm tp}, \\ 0, & \text{otherwise.} \end{cases} \tag{7}$$

$z_{\rm tp} = 12$ km is the tropopause height ($\sigma_{\rm tp}$ is the corresponding σ level), $L = 6.5\ \mathrm{K\,km^{-1}}$ is the vertical lapse rate, and $T_z^*|_{\rm tp} = T_0 - L z_{\rm tp}$ is the temperature at the tropopause, with $T_0 = 288$ K the globally-averaged surface temperature.

Configuration	$8\Omega_\mathrm{E}$	$4\Omega_\mathrm{E}$	$2\Omega_\mathrm{E}$	Ω_E	$\Omega_\mathrm{E}/2$	$\Omega_\mathrm{E}/4$	$\Omega_\mathrm{E}/8$	$\Omega_\mathrm{E}/16$	$\Omega_\mathrm{E}/32$	$\Omega_\mathrm{E}/64$	$\Omega_\mathrm{E}/128$	$\Omega_\mathrm{E}/256$	$\Omega_\mathrm{E}/512$
3D, T127	✓	✓	✓	✓		✓		✓		✓			
3D, T42				✓	✓	✓	✓	✓	✓	✓	✓	✓	✓
Axisymmetric		✓	✓	✓	✓	✓	✓	✓	✓	✓	✓		

TABLE 1. Rotation rates considered for each model configuration. $\Omega_\mathrm{E} = 7.29\times10^{-5}\,\mathrm{s}^{-1}$ is the Earth's rotation rate.

$\Delta T_h^* = 60\,\mathrm{K}$ is the equator-to-pole temperature difference at the surface. $K = 2$ K is a smoothing parameter that ensures a continuous temperature change across the tropopause. The radiative relaxation timescale is 2.5 days in the boundary layer ($\sigma > 0.8$), and 30 days in the free atmosphere.

The decision to use the relaxation temperature profile of Wang et al. (2018) was made so that we could perform comparisons between the results of experiments run using their model (PUMA) and those presented in this work (not shown). We have checked that the circulation obtained using this forcing is essentially identical to that obtained using the original Held and Suarez (1994) forcing, at both high and low rotation rates.

Drag and dissipation

A linear drag is applied in the boundary layer, operating on a timescale of 0.6 days, and in the upper-atmosphere ($\sigma < 0.01$, applied to the eddy components of the flow only), operating on a timescale of 0.5 days. The drag in the upper atmosphere is included as a sponge layer, to avoid the reflection of waves at the model top.

A hyperviscosity term is applied to the momentum and thermodynamic equations:

$$\frac{\partial \zeta}{\partial t} = \cdots + \nu \nabla^{2n} \zeta, \tag{8}$$

$$\frac{\partial D}{\partial t} = \cdots + \nu \nabla^{2n} D, \tag{9}$$

$$\frac{\partial T}{\partial t} = \cdots + \kappa \nabla^{2n} T, \tag{10}$$

operating on a timescale of 0.25 days at the grid scale. $n = 4$ is the damping order. ζ, D, and T are the vorticity, divergence, and temperature. This term is included to parametrise the dissipation of energy by sub-grid scale dynamics.

b. Description of model runs

We run GCM experiments over a wide range of rotation rates, from $8\Omega_\mathrm{E}$ to $\Omega_\mathrm{E}/512$, where $\Omega_\mathrm{E} = 7.29\times10^{-5}\,\mathrm{s}^{-1}$ is the Earth's rotation rate. All other planetary parameters are taken to be Earth-like: $a = 6.4\times10^{6}\,\mathrm{m}$, $g = 9.81\,\mathrm{m\,s^{-1}}$, and surface pressure $p_0 = 1\,\mathrm{bar}$.

Three-dimensional experiments are run at both T127 and T42 spectral resolution (corresponding to approximately 1° and 2.8° lat-lon resolution respectively, at the equator). We also run axisymmetric experiments, which are constructed by retaining only zonal wavenumber $m = 0$ coefficients in the spectral dynamical core at each time step. Axisymmetric experiments are run with the same meridional resolution as the T127 three-dimensional experiments. The specific rotation rates run in each configuration are shown in Table 1.

Each of the experiments is run to equilibrium, by which we mean that S is no longer evolving with time. In order to achieve this, three-dimensional experiments with $\Omega \geq \Omega_\mathrm{E}/4$ are run for 3 (Earth) years, the $\Omega = \Omega_\mathrm{E}/8$ experiment is run for 6 years, and experiments with $\Omega \leq \Omega_\mathrm{E}/16$ are run for 8 years. The axisymmetric experiments are all run for 3 years.

c. Data analysis

The 3D model data analysed in this paper is output in daily-averaged format, and the axisymmetric model data is output in monthly-averaged format. `Isca` outputs data on the σ coordinate vertical grid. We subsequently interpolate the data onto pressure levels $p_\ell = \sigma_\ell p_0$. Occasionally $p_\ell > p_s(t, \lambda, \vartheta)$, in which case the data is set to `NaN` (the grid-point being interpolated onto is below the surface). In order to correctly take account of these subterranean grid points when computing integrals and averages, we make use of the techniques described by Boer (1982).

3. Zonally-averaged circulations

To provide context for the rest of the paper, we begin the presentation of our experiment results by discussing some aspects of their zonally-averaged circulations. Each of the experiments discussed in this section was run at T127 resolution. We note that the structure of the circulation obtained in our numerical experiments, and the dependence of the circulation on rotation rate, is consistent with that presented in previous work [e.g., Dias Pinto and Mitchell (2014), Kaspi and Showman (2015), Wang et al. (2018), and Colyer and Vallis (2019)].

The zonal-mean zonal wind $\overline{u}$, and meridional mass streamfunction

$$\Psi(\vartheta, p) = 2\pi a \cos\vartheta \int_0^p \overline{v}\,\mathrm{d}p/g \tag{11}$$

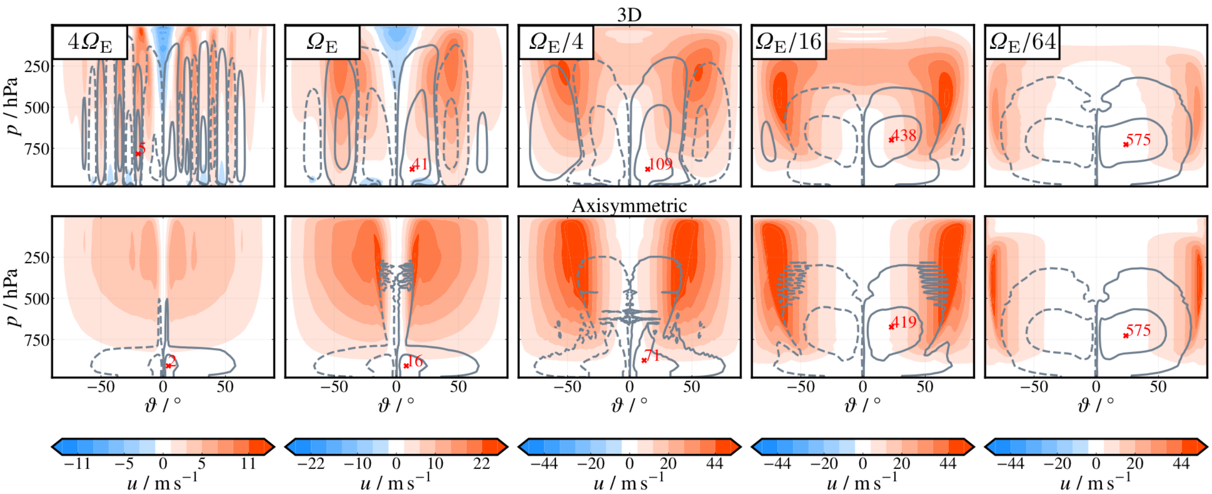

FIG. 1. Zonal-mean zonal wind u (colour), and meridional mass streamfunction Ψ (contours). All experiments shown were run with T127 horizontal resolution. The rotation rate for each experiment is indicated in the top-left corner of each panel. Note that the colour scale for u varies between panels. The red cross (and number) indicates the location (and value) where Ψ is maximum. The maximum value for Ψ has units $\times 10^9\,\mathrm{kg\,s^{-1}}$. The solid contours delimit 5% and 50% of the maximum, and the dashed contours show '$-1\times$' the solid contours. As the contour levels are percentages of the maximum value for Ψ, they vary between panels.

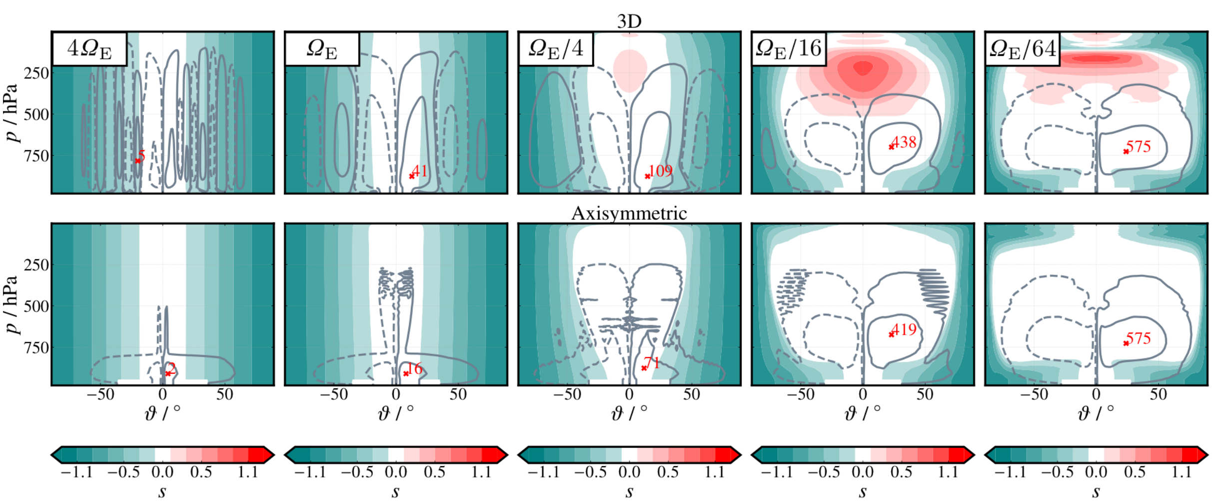

FIG. 2. Local super-rotation index, s. As in Figure 1, the red label and contours show the meridional mass streamfunction Ψ (see Figure 1 caption for details). All experiments shown were run with T127 horizontal resolution.

are shown in Figure 1 (colour for $\overline{u}$, contours for Ψ) for the 3D (top row) and axisymmetric (bottom row) T127 experiments. The zonally-averaged specific axial angular momentum, normalised by the planetary specific angular momentum at the equator,

$$s = \frac{\overline{m}}{\Omega a^2} - 1, \tag{12}$$

is shown in Figure 2 (colour), with Ψ once again overlaid for reference (contours). s is often referred to as the local super-rotation index (Read and Lebonnois 2018), and is defined such that $s \leq 0$ in an axisymmetric atmosphere (i.e., as $\overline{m} \leq \Omega a^2$). Where $s > 0$ the atmosphere may be termed 'locally super-rotating'.

In each of the experiments, thermally-direct Hadley cells which feature air rising at the equator and sinking at higher latitudes are present. The action of the Hadley cell to fill the domain with air with $\overline{m} \approx \Omega a^2$ (equilibrated with the equatorial surface) is clearly visible in the s field (Figure 2), where the structure of the sub-tropical jets in the $\overline{u}$ field (Figure 1) is replaced by a single region within the Hadley cell where $s \approx 0$. The Hadley cells are flanked by a sub-tropical jet associated with approximate angular momentum conservation within the poleward moving branch of each cell. In the axisymmetric experiments, the maximum sub-tropical jet velocity increases from the $4\Omega_{\rm E}$ simulation to the $\Omega_{\rm E}/16$ simulation, before decreasing when Ω is decreased further. This is consistent with axisymmetric theory, which predicts that the sub-tropical jet velocity should increase with decreasing Ω at high and moderate (similar to the Earth) rotation rates, as the poleward moving branch of the Hadley cell extends towards higher latitudes (Held and Hou 1980). Then, for low rotation rates, axisymmetric theory predicts that the sub-tropical jet velocity decreases proportionally with Ω at low rotation rate, when the Hadley cell (and hence the jet) has essentially been pushed as far poleward as possible (Hou 1984; Colyer and Vallis 2019). A similar trend may be identified for the sub-tropical jets in the 3D experiments.

3D experiments with $\Omega \geq \Omega_{\rm E}$ feature additional mid-latitude jets poleward of each sub-tropical jet (Figure 1). The mid-latitude jets are 'eddy driven', accelerated by Rossby waves generated by mid-latitude baroclinic instability, which converge momentum into their source region (Thompson 1980). As the rotation rate is increased from $\Omega_{\rm E}$ to $4\Omega_{\rm E}$, the number of eddy driven jets increases as the characteristic lengthscale of baroclinic instability decreases (Williams 1978; Lee 2005). As the mid-latitude jets present in the 3D experiments are eddy driven, they are absent in the axisymmetric experiments at the same rotation rate, which leads to a very different $\overline{u}$ field. However, when the zonal flow is displayed in terms of s (Figure 2), the 3D experiments appear very similar to the axisymmetric experiments, and the complex structure of the eddy driven jets is no longer present. For rapidly rotating planets, the 'relative' component of m ($m_r = u \times a\cos\vartheta$) is much smaller than the contribution to m from the background rotation of the planet ($m_p = \Omega a^2 \cos^2\vartheta$). Eddies are important for the local angular momentum *budget* (as $\partial m/\partial t = \partial m_r/\partial t$), but the absolute value of m is essentially set by m_p.

At rotation rates $\leq \Omega_{\rm E}/4$, a prograde (locally super-rotating) jet emerges at the equator in the 3D experiments (Figure 1). This is associated with planetary-scale tropical disturbances which converge momentum towards the equator (Mitchell and Vallis 2010), which are generated when $\mathcal{R}$ is increased to an $O(1)$ value (Wang and Mitchell 2014). Regions of local super-rotation ($s > 0$, Figure 2) can clearly be identified for the 3D experiments, while in the axisymmetric experiments, local super-rotation is no longer present, in accordance with Hide's theorem. In the super-rotating 3D experiments, s is only significantly positive in the region above the Hadley circulation. This is because within the Hadley cell, air ascending at the equator acts to communicate the effects of friction at the surface to the atmosphere aloft. The meridional extent of the super-rotating region is confined within the bounds of the Hadley circulation, indicating that momentum is only converged towards the equator from within the region where it is deposited by meridional overturning.

In the 3D experiments, the maximum (super-rotating) zonal wind velocity at the equator is found in the $\Omega_{\rm E}/16$ experiment ($28\,{\rm m\,s^{-1}}$). It is of interest to note that while equatorial velocities in the $\Omega_{\rm E}/4$ and $\Omega_{\rm E}/16$ experiments are similar (Figure 1), the maximum local super-rotation *relative* to the underlying planet is much weaker in the $\Omega_{\rm E}/4$ experiment when compared with the $\Omega_{\rm E}/16$ experiment (Figure 2). When the rotation rate is further decreased to $\Omega_{\rm E}/64$ the maximum velocity at the equator is reduced ($8\,{\rm m\,s^{-1}}$) (Figure 1). The trend for the maximum equatorial velocity to decrease as Ω is reduced at very low rotation rates is present in the T42 experiments at even slower rotation rate; the maximum equatorial velocity is $1.2\,{\rm m\,s^{-1}}$ at $\Omega_{\rm E}/256$, and just $0.4\,{\rm m\,s^{-1}}$ at $\Omega_{\rm E}/512$.

The generation of equatorial super-rotation in our experiments is associated with the phase-locking of Kelvin and equatorial Rossby waves, which induces an equatorward angular momentum flux (Mitchell and Vallis 2010). The eastward moving Kelvin waves are able to phase lock with westward moving equatorial Rossby waves, as the Rossby waves are situated within the sub-tropical jet, and so are Doppler shifted westward (Wang and Mitchell 2014). We suspect that equatorial super-rotation collapses at very low rotation rate because the waves are no longer able to phase-lock when the Doppler shifted frequency of the Rossby waves [essentially $u(\vartheta_{\rm H})/(a\cos\vartheta_{\rm H})$ (Wang and Mitchell 2014), where $\vartheta_{\rm H}$ is the Hadley cell extent (i.e. the sub-tropical jet maximum)] increases as the sub-tropical jet is pushed to higher and higher latitudes. A full analysis of the collapse of local super-rotation at very low rotation rate is beyond the scope of the present study and is left as a topic for future work.

4. Dependence of global super-rotation on rotation rate

a. *Results from numerical experiments*

We now turn our discussion towards the dependence of the global super-rotation index S on planetary rotation rate Ω. Figure 3 shows S vs. $\mathcal{R}$ for each of the experiments run for this work. We choose to present S as a function of $\mathcal{R}$ instead of Ω in order to make a cleaner comparison between our numerical experiments, and estimates of S for the real planets (Venus, Titan, Mars, the Earth). This is necessary as the real planets are of different sizes, in addition to having different rotation rates, and these parameters can be of similar dynamical importance [see Mitchell and Vallis (2010) and Dias Pinto and Mitchell (2014)]. The values used to calculate $\mathcal{R}$ for our numerical experiments and the real planets are provided in Table 2.

In both the 3D and the axisymmetric experiments, S ($S_{\rm 3D}$ and $S_{\rm ax}$, respectively) increases with decreasing Ω (increasing $\mathcal{R}$) when $\mathcal{R}$ is small (rapid rotation rate), and $S \ll 1$, which indicates that the dynamics are in a

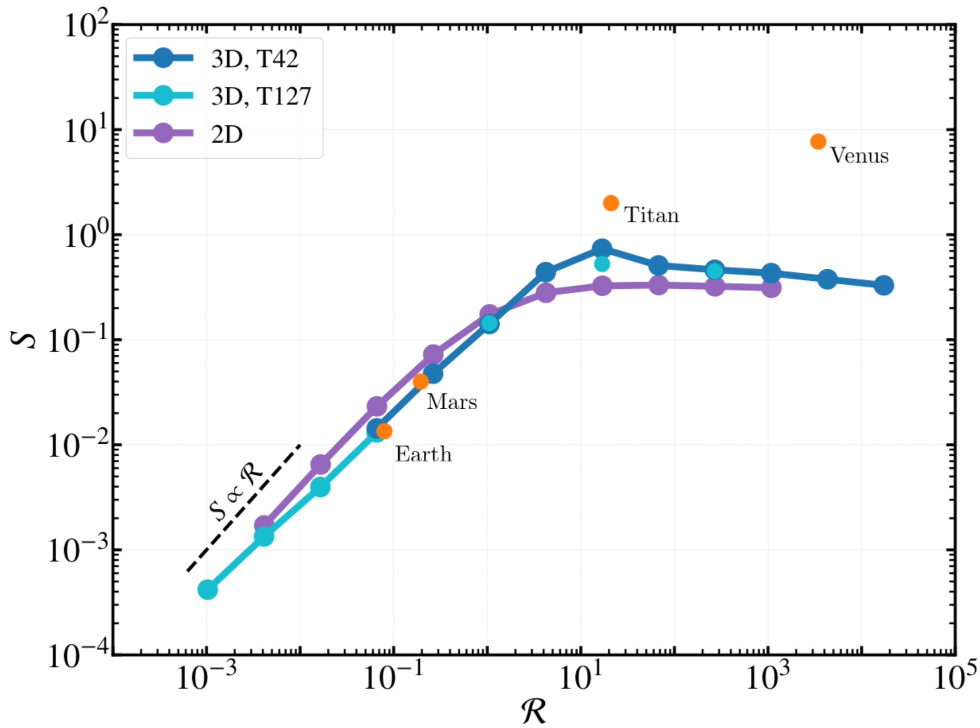

FIG. 3. Global super-rotation index S vs. thermal Rossby number $\mathcal{R}$. 3D experiments are shown in blue, and axisymmetric (2D) experiments in purple. Experiments run at T42 are plotted in dark blue, and those run at T127 are plotted in light blue. The orange dots show estimates for S for the Earth, Mars, Titan and Venus, and are taken from Read and Lebonnois (2018). The black dashed line indicates a Ω^{-2} scaling.

Planet	a	Ω	ΔT_{eq}	R_d	$\mathcal{R}$
Earth	6371	7.29×10^{-5}	60	287	0.08
Mars	3396	7.09×10^{-5}	60	188	0.19
Venus	6051	2.99×10^{-7}	60	188	3450
Titan	2575	4.56×10^{-6}	10	290	21
`Isca`	6400	variable	60	287	variable

TABLE 2. Parameter values used to calculate $\mathcal{R}$ for Figure 3. Units: km for a, s^{-1} for Ω , K for ΔT_{eq}, $\mathrm{J\,kg^{-1}\,K^{-1}}$ for R_d.

regime where the local momentum budget is dominated by geostrophic balance throughout the domain. When $\mathcal{R}$ is large (slow rotation rate), S saturates so that it becomes virtually independent of Ω (and $\mathcal{R}$). S saturates at a value $S < 1$, indicating that a regime where the atmospheric dynamics are dominated by cyclostrophic balance is not obtained – even for the 3D experiments. The sole exception to this is the 3D $\Omega = \Omega_E/16$ experiment (T42 resolution), for which S is close to unity.

For the axisymmetric experiments, S_{ax} appears to scale inversely with Ω^2 when $\mathcal{R}$ is small; this may be inferred by comparing the black dashed line (Ω^{-2}) with the solid purple line. At high $\mathcal{R}$, S_{ax} appears to saturate at a value $S_{ax} \approx 0.3$. This is less than the limiting value of $S_{ax} = 1/2$ for an axisymmetric atmosphere.

The normalised difference $\Delta S = (S_{3D} - S_{ax})/S_{ax}$ (shown in Figure 4) between S_{3D} and S_{ax} is generally $|\Delta S| < 1$, with the exception of the $\Omega_E/16$ T42 experiment, for which $\Delta S = 1.25$. For the T127 experiments, ΔS is maximal when $\Omega = \Omega_E/16$, for which $\Delta S = 0.61$, and minimal (most negative) when $\Omega = \Omega_E$, for which $\Delta S = -0.43$. The values taken by S_{3D} appear to be perturbations around S_{ax} (i.e., S in each case is of the same order of magnitude). In our idealised model, eddies are unable to substantially modify the globally integrated atmospheric angular momentum away from that realised in axisymmetric setting.

When $\mathcal{R}$ is small, S_{3D} is less than S_{ax}, and when $\mathcal{R}$ is large, S_{3D} is greater than S_{ax}. Each of the numerical experiments is initiated with $u = 0$ everywhere, corresponding to $S = 0$, and so the equilibrium value of S is a measure of the total zonal angular momentum injected into the atmosphere during spin-up; $\mathrm{d}S/\mathrm{d}t = 0$ when the globally integrated surface stress $\mathcal{T} = 0$. Figure 5 shows S as function of time over the first 120 days of the $\Omega = \Omega_E$ experiment, and the first 360 days of the $\Omega = \Omega_E/16$ experiment (both T127 resolution). For both experiments shown, S_{3D} and S_{ax} are initially nearly identical. During this initial period, angular momentum is lifted into the atmosphere by the mean flow, and there is little vertical momentum transport due to

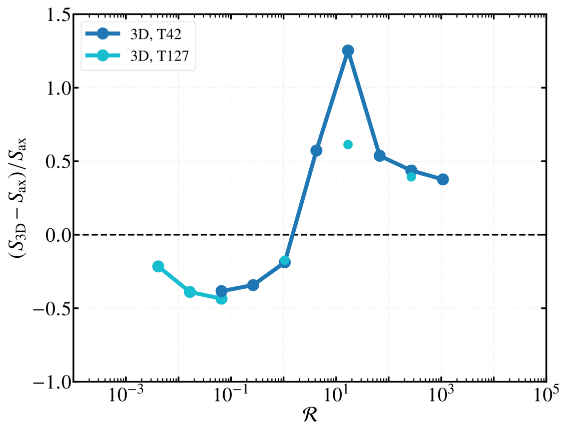

FIG. 4. Difference between S_{3D} and S_{ax}, normalised by S_{ax}. The shade of blue indicates the resolution of the 3D experiment. All axisymmetric experiments were run with meridional resolution equivalent to the T127 3D experiments.

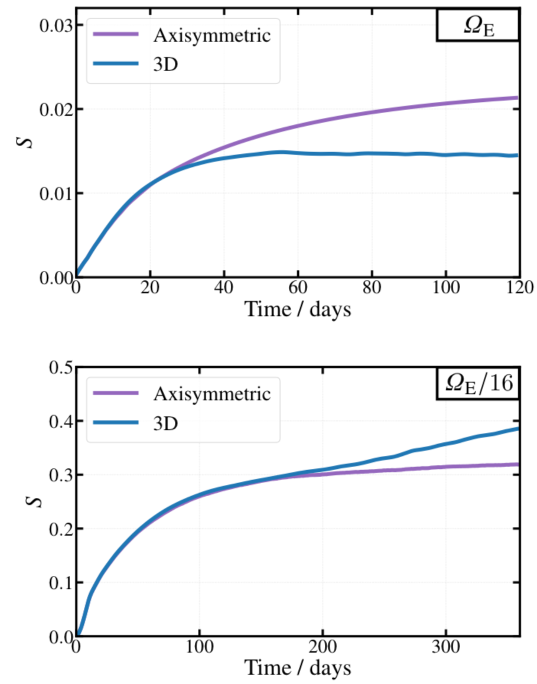

FIG. 5. S vs. t for axisymmetric and 3D experiments. Top panel: S vs. t for the first 120 days of the Ω_E experiments. Bottom panel: S vs. t for the first 360 days of the $\Omega_E/16$ experiments. Blue curves show 3D experiments and purple curves show axisymmetric experiments. All output shown is from experiments with T127 resolution.

eddy activity. After day 30 for the $\Omega = \Omega_E$ experiment, and day 180 for the $\Omega = \Omega_E/16$ experiment, non-axisymmetric disturbances cause S_{3D} and S_{ax} to diverge. For the $\Omega_E/16$ case, eddies which induce an up-gradient transport of m allow the mean flow to lift more angular momentum into the atmosphere by removing angular momentum from the descending branch of the Hadley circulation and depositing it at the equator (Gierasch 1975). This leads to $S_{3D} > S_{ax}$. For the Ω_E case, Rossby waves generated by baroclinic instability induced a down-gradient transfer of m into the boundary layer (Andrews et al. 1983), which counteracts upward transport of m by the mean flow. This causes the Ω_E experiment to equilibrate with $S_{3D} < S_{ax}$.

The difference between the 3D and axisymmetric experiments $|\Delta S|$ is largest for intermediate values of $\mathcal{R} \approx 0.1$ – 10. When $\mathcal{R} \ll 1$ and $\mathcal{R} \gg 1$ (i.e., at very high *and* very low rotation rate) S_{3D} converges towards S_{ax}. This is consistent with a decrease in the characteristic scale of baroclinic instability as the rotation rate increased in the $\mathcal{R} \ll 1$ regime (Lee 2005; Schneider and Walker 2008), and the collapse of the instability generating local super-rotation when the rotation rate is decreased in the $\mathcal{R} \gg 1$ regime (see discussion at the end of Section 3).

Estimates of S for the Earth, Mars, Venus, and Titan [taken from Read and Lebonnois (2018)] are shown as orange dots in Figure 3. The 3D experiments with $\mathcal{R}$ closest to the Earth (Ω_E) and Mars ($\Omega_E/2$) obtain values for S similar to those obtained by the two real planets. At low rotation rate, however, experiments with $\mathcal{R}$ characteristic of Venus ($\Omega_E/128$) and Titan ($\Omega_E/16$) do not generate global super-rotation of a similar order of magnitude to that estimated for the real planets (particularly for Venus), indicating that the processes responsible for storing excess m in the atmospheres of Venus and Titan are not (fully) represented in our *Earth-like* numerical model.

b. Theory for S in axisymmetric case

In this section, we would like to understand which processes contribute to the $\mathcal{R} \ll 1$ and $\mathcal{R} \gg 1$ scalings for S obtained in our numerical experiments (Figure 3). To do so, we will develop a theory for S in terms of $\mathcal{R}$, for the case of an axisymmetric, inviscid atmosphere, based on the model of Held and Hou (1980).

The Held–Hou model

Held and Hou (1980, hereafter HH) present an analytic model for the circulation of an axisymmetric atmosphere in the inviscid limit, derived from the Boussinesq approximation of the hydrostatic primitive equations.

The HH model consists of essentially two layers, a lower layer with $u \approx 0$, and an upper layer (the free atmosphere) where $u(\vartheta, z) \neq 0$ and is in gradient wind balance with the model temperature field

$$\frac{\partial}{\partial z}\left(fu + \frac{u^2 \tan\vartheta}{a}\right) = -\frac{g}{a\theta_0}\frac{\partial \theta}{\partial \vartheta}, \qquad (13)$$

where g is the acceleration due to gravity, θ_0 is the mean surface temperature, and θ is the potential temperature. The advective term which would appear on the left-hand-side of (13) is assumed to be small and has been omitted.

The atmospheric circulation is forced by a linear relaxation to a radiative-convective equilibrium potential temperature field θ_{eq}

$$\frac{\theta_{\mathrm{eq}}}{\theta_0} = 1 - \frac{2}{3}\Delta_h P_2(\sin\vartheta) + \Delta_v\left(\frac{z}{H} - \frac{1}{2}\right) \tag{14}$$

where $\theta_0\Delta_h$ is the equator-to-pole surface temperature difference, $P_2(x) = (3x^2 - 1)/2$ is the second Legendre polynomial, and $\theta_0\Delta_v$ is the vertical potential temperature difference between the surface and the top of the domain.

(13) and (14) may be vertically integrated to yield

$$fu + \frac{u^2\tan\vartheta}{a} = -\frac{gH}{a\theta_0}\frac{\partial\overline{\theta}}{\partial\vartheta} \tag{15}$$

at $z = H$, and

$$\overline{\theta}_{\mathrm{eq}} = \theta_0\left[1 - \frac{2}{3}\Delta_h P_2(\sin\vartheta)\right], \tag{16}$$

where here an overline denotes a vertical average $H^{-1}\int_0^H \mathrm{d}z$, and H is the domain height.

In the free atmosphere, the circulation is divided into two regions: a tropical (or Hadley cell) region, and an extra-tropical region. In the extra-tropical region, $v = 0$, so u is determined through gradient wind balance by the radiative-convective equilibrium temperature field [i.e. $\theta = \theta_{\mathrm{eq}}$ in (13)], and takes the form

$$u_{\mathrm{ET}} = \Omega a\cos\vartheta\left(\sqrt{2\mathcal{R}\frac{z}{H} + 1} - 1\right), \tag{17}$$

where $\mathcal{R} \equiv (\Delta_h gH)/(\Omega a)^2$ is the analogue of (1) for the Boussinesq equations [see Appendix A of Colyer and Vallis (2019) for a discussion regarding the correspondence between $\mathcal{R}$ in the Boussinesq and non-Boussinesq primitive equations].

In the upper level of the Hadley cell region, u is determined by conservation of specific axial angular momentum m. Air is assumed to rise at the equator with $u = 0$, and u depends on ϑ as

$$u_{\mathrm{HC}} = \frac{\Omega a\sin^2\vartheta}{\cos\vartheta}. \tag{18}$$

The vertically averaged potential temperature field in the Hadley cell region is then determined to be in gradient wind balance with u_{HC} [i.e. $u = u_{\mathrm{HC}}$ in (15)]:

$$\frac{\overline{\theta}(0) - \overline{\theta}}{\theta_0} = \frac{u_{\mathrm{HC}}^2}{2gH}. \tag{19}$$

HH then solve for the Hadley cell boundary latitude ϑ_{H} by enforcing two matching conditions:

$$\overline{\theta}\left(\vartheta_{\mathrm{H}}^{+}\right) = \overline{\theta}\left(\vartheta_{\mathrm{H}}^{-}\right), \tag{20}$$

and

$$\int_0^{\vartheta_{\mathrm{H}}} \overline{\theta}\cos\vartheta\,\mathrm{d}\vartheta = \int_0^{\vartheta_{\mathrm{H}}} \overline{\theta}_{\mathrm{eq}}\cos\vartheta\,\mathrm{d}\vartheta. \tag{21}$$

(20) requires that potential temperature be continuous across the Hadley cell boundary, and (21) requires that the Hadley cell is thermodynamically closed.

If (16) and (19) are substituted into (21), then (20) and (21) may be used to derive the following expression

$$\mathcal{R} = \frac{3}{4}\left[\frac{1}{3} + \frac{1}{x_{\mathrm{H}}^2} + \frac{x_{\mathrm{H}}^2}{1 - x_{\mathrm{H}}^2} - \frac{1}{2x_{\mathrm{H}}^3}\ln\left(\frac{1 + x_{\mathrm{H}}}{1 - x_{\mathrm{H}}}\right)\right] \tag{22}$$

where $x_{\mathrm{H}} = \sin\vartheta_{\mathrm{H}}$, which may be solved numerically for ϑ_{H} given $\mathcal{R}$ (defined in terms of external parameters).

Expression for S

In order to relate S to $\mathcal{R}$, we will make use of the zonal velocity profiles found for the tropical and extra-tropical regions of the HH model. We will assume

$$u = \begin{cases} u_{\mathrm{HC}}, & \vartheta \in [0, \vartheta_{\mathrm{H}}], \\ u_{\mathrm{ET}}, & \vartheta \in (\vartheta_{\mathrm{H}}, \pi/2]. \end{cases} \tag{23}$$

u_{HC} is given by (18) for all $p/p_s < 0.8$ (i.e., in the free atmosphere), and $u_{\mathrm{HC}} = 0$ in the boundary layer. u_{ET} is given by (17) through the depth of the atmosphere. By assuming that u_{HC} is independent of z in the free atmosphere, we are assuming that, above the boundary layer, $\partial\theta/\partial\vartheta \to 0$ within the Hadley cell (Fang and Tung 1999).

We note that in our numerical simulations, the Hadley cell boundary contracts inwards with decreasing altitude, and consequently so does the region where $u = u_{\mathrm{HC}}$. Our choice for u_{HC} may lead to an overestimate of S, although this overestimate will likely be small, as the Hadley cell width exhibits a weak altitude dependence above 800 hPa in the majority of our experiments (see the boundary of the white contour in Figure 2).

The definition of S may be re-written

$$S = \frac{\int \rho a\cos\vartheta\, u\,\mathrm{dV}}{\int \rho\Omega a^2\cos^2\vartheta\,\mathrm{dV}}, \tag{24}$$

as the -1 in (2) cancels with the planetary ($\Omega a^2\cos^2\vartheta$) contribution to m in the numerator. S may then be split into contributions from the Hadley cell and extra-tropical regions

$$S = S_{\mathrm{HC}} + S_{\mathrm{ET}} \tag{25}$$

where

$$S_{\mathrm{HC}} = \frac{\int_0^{\frac{4}{5}p_s}\int_0^{\vartheta_{\mathrm{HC}}} u_{\mathrm{HC}}\cos^2\vartheta\,\mathrm{d}\vartheta\,\mathrm{d}p/g}{\int_0^{p_s}\int_0^{\frac{\pi}{2}} \Omega a\cos^3\vartheta\,\mathrm{d}\vartheta\,\mathrm{d}p/g}, \tag{26}$$

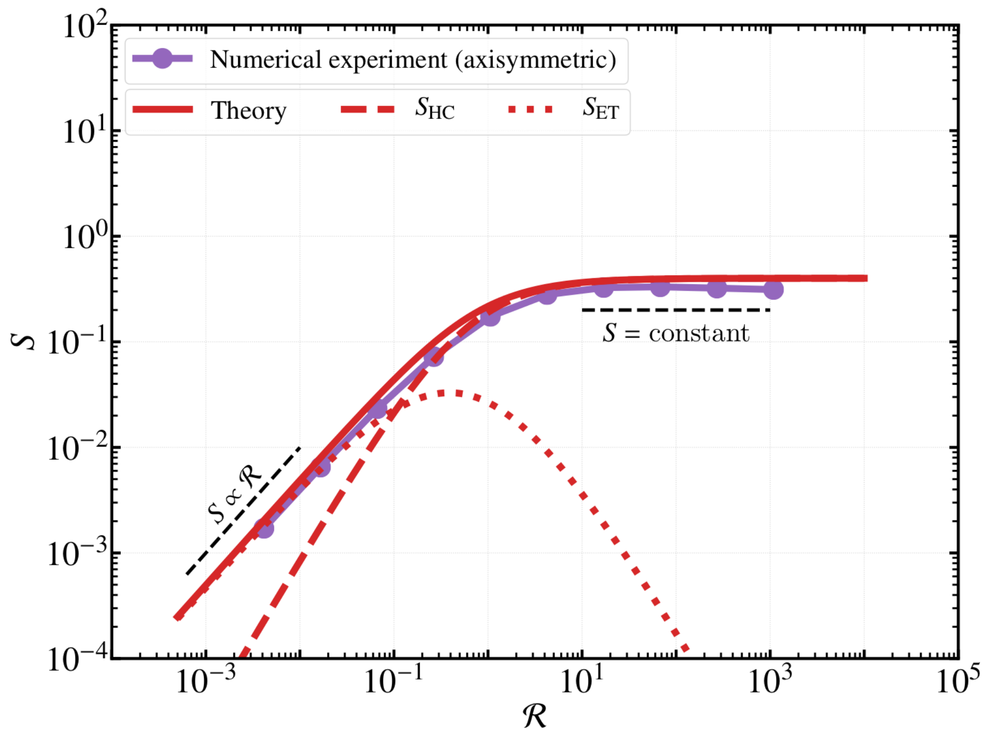

FIG. 6. Theoretical prediction for S from (28) vs. $\mathcal{R}$ for the case of an axisymmetric atmosphere (solid red curve). Also shown are the contributions to the theoretical S from the Hadley cell and extra-tropical regions, S_{HC} and S_{ET}. The purple line shows S for the axisymmetric numerical experiments.

and,

$$S_{\mathrm{ET}} = \frac{\int_0^H \int_{\vartheta_{\mathrm{HC}}}^{\frac{\pi}{2}} u_{\mathrm{ET}} \cos^2\vartheta \,\mathrm{d}\vartheta \,\rho_0 \mathrm{d}z}{\int_0^H \int_0^{\frac{\pi}{2}} \Omega a \cos^3\vartheta \,\mathrm{d}\vartheta \,\rho_0 \mathrm{d}z}. \tag{27}$$

Note that in the Boussinesq framework, $\rho = \rho_0$ is a constant reference density, and we have used hydrostatic equilibrium $\mathrm{d}p = -g\rho_0 \mathrm{d}z$ to write (26) as an integration over pressure. The integration $\int \mathrm{d}\lambda$ in each expression cancels between the numerator and denominator due to axisymmetry, and is omitted.

(26) and (27) may then be evaluated analytically using (18) and (17) to obtain

$$\begin{aligned} S &= S_{\mathrm{HC}} + S_{\mathrm{ET}} \\ &= \frac{2}{5}\sin^3\vartheta_{\mathrm{H}} + \\ &\quad \frac{1}{12}\left[\frac{(2\mathcal{R}+1)^{\frac{3}{2}}-1}{2\mathcal{R}} - \frac{3}{2}\right](8 - 9\sin\vartheta_{\mathrm{H}} - \sin 3\vartheta_{\mathrm{H}}). \end{aligned} \tag{28}$$

As ϑ_{H} depends only on $\mathcal{R}$ [obtained by solving (22)], S is now determined solely by $\mathcal{R}$.

c. Comparison between theoretical S and simulation results

S predicted by (28) is plotted against $\mathcal{R}$ in Figure 6. The values for S calculated for the axisymmetric numerical experiments are also shown, and there is good agreement between the theoretical prediction for S and the numerical experiments in both the high and low rotation rate limits. For intermediate $\mathcal{R}$, the theoretical prediction for S is a slight overestimate of that obtained in the numerical experiments; this is due to our simplifying assumption that ϑ_{H} is independent of height, which is most strongly violated by experiments with intermediate $\mathcal{R}$ (see, for example, the $\Omega_{\mathrm{E}}/4$ experiment in Figure 2).

(28) is comprised of two terms, one that measures the contribution to S from the Hadley cell region (S_{HC}), and one that measures the contribution from the extra-tropical region (S_{ET}). These are shown in Figure 6 as a dashed and dotted curve, respectively. At high rotation rates, the extra-tropical term dominates the total value of S, as in this regime the Hadley cell is small and the 'extra-tropics' essentially comprise the whole atmosphere. At low rotation rates, the contribution to S from the Hadley cell dominates, as the Hadley cell expands to fill the domain. The transition between the extra-tropical and Hadley-cell dominated regimes occurs when the first and second terms in (28)

are equal. This occurs when $\mathcal{R} = 0.11$, corresponding to a Hadley cell latitude $\vartheta_{\mathrm{H}} = 22.8°$.

It is instructive to consider the behaviour of the axisymmetric theory in the limits $\mathcal{R} \ll 1$ and $\mathcal{R} \gg 1$. When $\mathcal{R} \ll 1$ (rapid rotation)

$$\frac{(2\mathcal{R}+1)^{\frac{3}{2}} - 1}{2\mathcal{R}} - \frac{3}{2} \approx \frac{3\mathcal{R}}{4} \tag{29}$$

(via Taylor expansion). Additionally $\vartheta_{\mathrm{H}} \to 0$, meaning that $\sin\vartheta_{\mathrm{H}}$, $\sin 3\vartheta_{\mathrm{H}}$, and $\sin^3\vartheta_{\mathrm{H}} \to 0$. We then have

$$S \approx \frac{1}{2}\mathcal{R}. \tag{30}$$

In the rapidly rotating regime, S is dominated by the extra-tropical region (as the Hadley Cell is small), and (30) predicts that S scales linearly with $\mathcal{R}$, which corresponds to a Ω^{-2} scaling with rotation rate.

The $\mathcal{R}$ dependence in (28) comes from the expression for u_{ET}, (17), which originally derives from enforcing gradient wind balance in the extra-tropical region with the radiative-convective equilibrium forcing profile. This tells us that the $S \propto \Omega^{-2}$ scaling in the rapidly rotating regime is simply that implied by geostrophic thermal wind balance, which in this scenario is the dominant dynamical balance throughout the domain.

When $\mathcal{R} \gg 1$ (slow rotation) then $\vartheta_{\mathrm{H}} \to \pi/2$, so that $\sin\vartheta_{\mathrm{H}}$ and $\sin^3\vartheta_{\mathrm{H}} \to 1$, while $\sin 3\vartheta_{\mathrm{H}} \to -1$. In this scenario, the axisymmetric theory approaches

$$S \approx \frac{2}{5} = \text{const.} \tag{31}$$

The $\mathcal{R} \gg 1$ limit is the scenario where the Hadley cell has filled the entire domain. This is qualitatively the same as the $S = 1/2$ limit suggested in Section 1, and the additional factor $4/5$ comes from assuming $u = 0$ in the boundary layer ($p/p_{\mathrm{s}} > 0.8$). In this limit, the entire free atmosphere has specific zonal angular momentum $m = \Omega a^2$ due to the equilibration of air with the equatorial surface, and conservation of m in the free atmosphere. In this scenario, the dominant term in the local momentum budget varies through the domain; at low latitudes, geostrophic balance is dominant, and at middle and high latitudes, cyclostrophic balance dominates. This may be appreciated by considering the ratio of the cyclostrophic and geostrophic terms in (13) when $u = u_{\mathrm{HC}}$, i.e., $u_{\mathrm{HC}} \tan\vartheta/(2\Omega a \sin\vartheta) = \tan^2\vartheta/2$, which is greater than one (indicating the local dominance of cyclostrophic balance) when $\vartheta > 54.7°$, and less than one otherwise (indicating local dominance of geostrophic balance).

In summary, the results from our theoretical model suggest that in our axisymmetric experiments, the dependence of S on $\mathcal{R}$ at high rotation rate is determined by geostrophic thermal wind balance, while at low rotation rate, it is determined by approximate conservation of angular momentum. The presence of eddies does not alter the dependence of S on $\mathcal{R}$ obtained in our 3D experiments from that in the axisymmetric experiments, at least to first order (see Section 4 a), and so it is likely that the same processes also determine the $\mathcal{R} \ll 1$ and $\mathcal{R} \gg 1$ behaviour of S in the 3D model.

5. Discussion

a. Relationship between S and circulation regime

Part of the motivation for studying S is due to its similarity with a zonal Rossby number, which means that the value of S is indicative of the dynamical regime occupied by a planetary atmosphere (Read 1986a).

By considering the limits of our axisymmetric theory for S, we have shown that the relationship between S and circulation regime is manifest in the local dependence of S on $\mathcal{R}$. In the rapid rotation rate limit, $S \propto \mathcal{R} \ll 1$ defines a regime where geostrophic balance is dominant in the local momentum budget, throughout the atmosphere. At low rotation rate, $S = \text{constant}$ defines a regime where the dynamics are determined by approximate conservation of angular momentum within the Hadley circulation, which fills the domain at low rotation rate, and the local momentum budget is characterised by a mixed gradient wind balance.

As discussed in the introduction, $S \gg 1$ indicates a further regime, characteristic of the atmospheres of Venus and Titan, where the local momentum budget is dominated by cyclostrophic balance throughout the domain. We are not able to comment on the cyclostrophic regime within the framework provided by our axisymmetric theory; $S > 1/2$ requires some representation of up-gradient angular momentum transport, and is not obtainable in an axisymmetric, inviscid model. However, we can draw on the results of Yamamoto and Yoden (2013, hereafter YY), who derive an expression for a non-dimensional measure of super-rotation strength $S' = 4S/3$ (see Appendix A) in terms of $\mathcal{R}$,

$$\left[S'^2 + 2S' + BS'\left(\frac{2+S'}{1+S'}\right)\right]\left[\frac{AS'}{2}\left(\frac{2+S'}{1+S'}\right)+1\right] = 2\mathcal{R}, \tag{32}$$

derived from the Boussinesq primitive equations on a sphere forced by Newtonian relaxation (e.g., as in HH and in this work), *in the presence of diffusion of angular velocity*. S depends on the external parameters A, B, and $\mathcal{R}$. $\mathcal{R}$ is the same as in our axisymmetric theory, and $A = \pi^2\tau/\tau_{\mathrm{V}}$ and $B = 20\pi^2\left(\Omega^{-1}/\sqrt{\tau_{\mathrm{H}}\tau_{\mathrm{V}}}\right)^2$, where τ is the radiative relaxation timescale, τ_{V} is the timescale for vertical eddy momentum diffusion, and τ_{H} is the timescale for horizontal eddy momentum diffusion. In the YY theory, diffusion terms are formulated in analogy with molecular viscosity and so can transport angular momentum up-gradient (Read 1986b). YY assume that the relaxation time for horizontal diffusion is much shorter than the turnover time of the

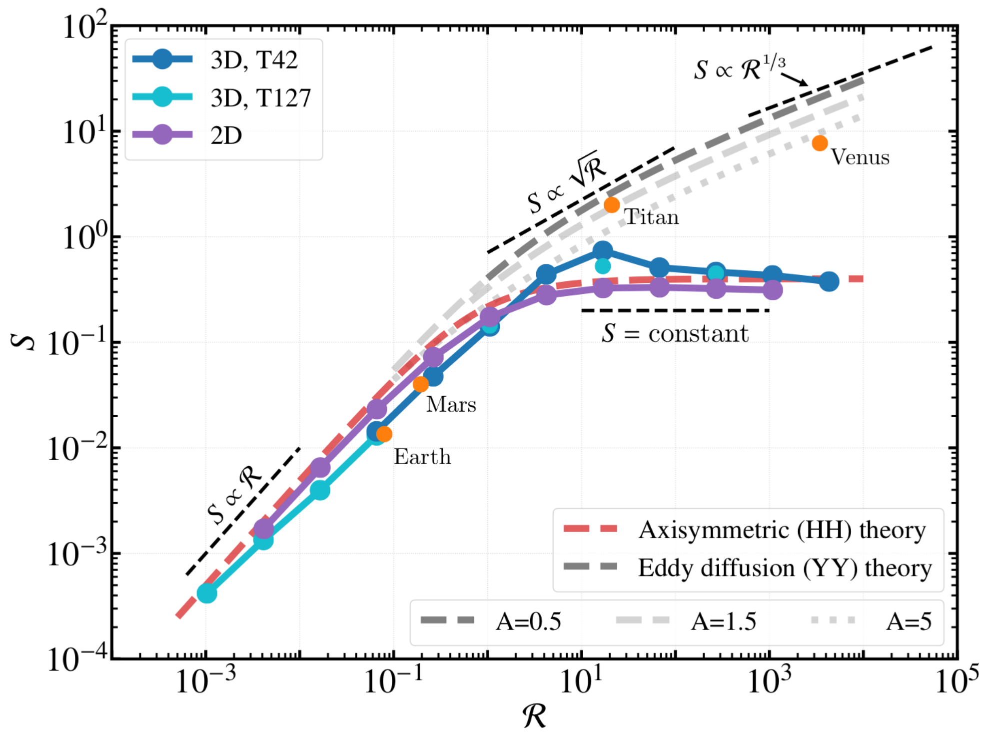

FIG. 7. S vs. $\mathcal{R}$ calculated from numerical experiments (solid curves) and theoretical predictions (dashed curves). 3D experiments are shown in blue, and axisymmetric experiments in purple (see Figure 3 caption for details). The orange dots show estimates for S for the Earth, Mars, Titan and Venus taken from Read and Lebonnois (2018). The red dashed curve shows S predicted by the axisymmetric theory (28). The grey dashed curves show S predicted by the quasi-axisymmetric theory of Yamamoto and Yoden (2013, our Eq. 32). In the YY theory, S depends on parameters A and B in addition to $\mathcal{R}$. Parameter values for A are shown in the legend, and B is set to $B = 0.3$ (see text for a definition of A and B, and justification of the values we choose for each). We only show S from the YY theory for $\mathcal{R} > 0.1$. This choice is made both to enhance the clarity of the figure (for $B = 0.3$ the YY curves are essentially identical to ours when $\mathcal{R} \ll 1$), and because, when $\mathcal{R} \ll 1$, it is difficult to place a physical interpretation on the circulation implied by the YY theory due to the assumption of strong horizontal diffusion [see footnote 2 in the text, and Section 5.5 of Yamamoto and Yoden (2013)].

meridional circulation, and the relaxation time for vertical diffusion, which allows the YY theory to access the cyclostrophic regime where $S \gg 1$, occupied by Titan and Venus.

S predicted by the YY theory is shown in Figure 7 alongside values for S computed from our axisymmetric, inviscid theory (Section 4 b and Section 4 c) and our numerical experiments (Section a). We only show S from the YY theory for $\mathcal{R} > 0.1$, as when $\mathcal{R} \ll 1$ it is generally no longer appropriate to assume up-gradient eddy angular momentum transport. Multiple curves are shown, with different curves corresponding to different values for A. The values for A are chosen to be in the 'correct ballpark' for Venus and Titan (see Section 5.5 of YY), and multiple values are shown to demonstrate the dependence of S on A. For all YY curves, we set $B = 0.3$. The parameter B is only important in determining the behaviour of S at low and intermediate $\mathcal{R}$ (high and intermediate rotation rate), and has no effect on the $\mathcal{R} \gg 1$ asymptote. $B < 1$ puts the curves in the geostrophic regime occupied by our numerical experiments, the Earth, and Mars, and the $B = 0.3$ is chosen so that the YY curves join up with our axisymmetric theory at approximately $\mathcal{R} = 0.1$.

YY show that for intermediate values for $\mathcal{R}$, $1 < \mathcal{R} < 10$, S scales with $\sqrt{2\mathcal{R}} \propto \Omega^{-1}$, which corresponds to either (i) a scaling associated with the dominance of cyclostrophic balance in the local momentum budget, or (ii) a scaling associated with the dominance of geostrophic balance, modified from $S \propto \mathcal{R}$ (i.e., the scaling in our theory) to $S \propto \sqrt{\mathcal{R}}$. This modified-geostrophic scaling arises due to a significant reduction in the equator-to-pole temperature difference ΔT with respect to its radiative equilibrium value ΔT_{eq}. Regime (i) is realised when the timescale for vertical eddy momentum diffusion τ_{V} is much longer than the radiative relaxation time τ, $\tau_{\mathrm{V}} \gg \tau$, while regime (ii) corresponds to the opposite scenario where $\tau_{\mathrm{V}} \ll \tau$. For large $\mathcal{R} > 10$ ($S \gg 1$), S scales with $\mathcal{R}^{1/3} \propto \Omega^{-2/3}$, indicating a modified-cyclostrophic regime (again, due to a reduction in ΔT with respect to ΔT_{eq}).

Strong up-gradient angular momentum transport allows the YY theory to access the cyclostrophic regime, but it precludes their theory the angular momentum conserving regime occupied by our numerical experiments. Additionally, the strong-diffusion assumption makes it difficult to place a physical interpretation on the behaviour of the YY theory when $\mathcal{R} \ll 1$[2] (not shown in Figure 7). However, when our theory for the axisymmetric, inviscid case, is taken in tandem with the YY theory, the full breadth of dynamical regimes accessed by our numerical experiments and the real planets is captured.

Figure 7 makes clear the utility of S for characterising and comparing the dynamical regimes occupied by different atmospheres. The Earth and Mars clearly occupy the geostrophic regime defined by $S \ll 1$ and $S \propto \mathcal{R}$, while Titan and Venus clearly occupy the modified-geostrophic or cyclostrophic regimes for which $S \gg 1$ and $S \propto \sqrt{\mathcal{R}}$ or $S \propto \mathcal{R}^{\frac{1}{3}}$. It is also apparent that the regime towards which our Earth-like atmospheric model asymptotes when $\mathcal{R} \gg 1$, defined by $S = \text{constant} \approx 1/2$, is fundamentally different from that occupied by Venus and Titan. Figure 7 shows that the circulation regime associated with a given value of $\mathcal{R}$ is degenerate when $\mathcal{R}$ is made large. This is due to the high sensitivity of the atmospheric circulation to other input parameters in the slowly rotating regime (as discussed in the introduction, cf. Dias Pinto and Mitchell 2014). Unlike the thermal Rossby number $\mathcal{R}$, the combination of the value of S and the local dependence of S on $\mathcal{R}$ uniquely define the circulation regime occupied by a planetary atmosphere.

b. A 'default' regime for slowly rotating (large $\mathcal{R}$) planets?

Low planetary rotation rate, or more generally, large $\mathcal{R}$, is commonly taken to imply a dynamical regime characterised by cyclostrophic balance and strong equatorial super-rotation, which in terms of S is the regime where $S \gg 1$ (e.g., Read 2011; Showman et al. 2013; Held 2018). This assumption is partly influenced by the observation of strong global super-rotation in the atmospheres of Venus and Titan, and additionally because local super-rotation has been shown to emerge in idealised 'Earth-like' numerical models when $\mathcal{R}$ is made large [e.g. Mitchell and Vallis (2010)].

However, the circulations obtained from the numerical experiments presented in this work indicate that the degree of global super-rotation in an Earth-like atmosphere may saturate before reaching a strength comparable to that in Venus' and Titan's atmospheres. In our experiments, the non-axisymmetric disturbances that maintain equatorial super-rotation collapse at low rotation rate, and the atmospheric circulation approaches an axisymmetric state where it enters an angular momentum conserving regime, as opposed to the cyclostrophic regime occupied by Venus and Titan. This is consistent with previous work (Dias Pinto and Mitchell 2014), which has shown that strong super-rotation does not necessarily emerge in an Earth-like atmosphere at low rotation rate. Furthermore, Lu and Yamamoto (2020) have shown that the stronger super-rotation obtained in Earth-like simulations with small planetary radius, such as those presented in Mitchell and Vallis (2010), Potter et al. (2014) and Dias Pinto and Mitchell (2014), may be sensitive to the strength of parametrised horizontal diffusion in these models (with weaker diffusion leading to weaker super-rotation).

Based on the results from our numerical experiments, those presented in previous work, and the different limiting behaviours of our axisymmetric, inviscid theory for S, and the YY theory, we conclude that it is not necessarily appropriate to assume that cyclostrophic balance and strong equatorial super-rotation are 'default' characteristics of a slowly rotating atmosphere (as is common), as both are clearly sensitive to other parameters and atmospheric processes. For example, Venus' strong global super-rotation is strongly sensitive to the existence of diurnal and semi-diurnal tides, excited due to its long solar day and substances in the atmosphere that absorb at UV wavelengths (Sánchez-Lavega et al. 2017). If these features are removed in a numerical model, then much weaker super-rotation is generated (Lebonnois et al. 2010). For Titan, the source of strong super-rotation is less clear, although it may be related (Williams 2006) to the fact that Titan's stratosphere, where super-rotation is strongest, is strongly statically stable (Fulchignoni et al. 2005; Flasar and Achterberg 2009).

6. Summary

In this work, we have studied the dependence of global super-rotation on planetary rotation rate using a combination of numerical and theoretical modelling. Our aim was to investigate the utility of the global super-rotation index S for characterising and comparing the circulation regimes occupied by different planetary atmospheres. Our results are summarised graphically in Figure 7.

We studied the dependence of S on Ω using an idealised Earth-like general circulation model in both 3D and axisymmetric configurations (Figure 3). In both configurations, we find that for $\mathcal{R} \ll 1$ (rapid rotation rate) $S \ll 1$, and S increases as Ω is decreased. When Ω is decreased

[2]The YY theory does have a geostrophic regime for $\mathcal{R} \ll 1$ where $S \propto \mathcal{R}$ (if additionally $B \ll 1$), but the implied circulation structure is quite different from that assumed by our theory. While the u wind profiles are similar (see Fig. 3 of YY), the structure of meridional overturning is different due to the assumed importance of horizontal diffusion. Even at high rotation rate, a single Hadley cell spans each hemisphere (see, e.g., the left-most columns Fig. 4 in YY). This feature of the circulation in the YY theory, combined with the sensitivity of the YY theory to the parameter B, make it difficult to place physical interpretation on its behaviour when $\mathcal{R} \ll 1$. In particular, in our theory the transition from the geostrophic to angular momentum conserving scaling for S is associated *the expansion* of the Hadley cell region (and contraction of the extra-tropical region). In the YY theory, where the Hadley cell always spans each hemisphere, the physical interpretation of the transition away from the geostrophic regime is less clear. The limitations of the YY theory when $\mathcal{R} \ll 1$ are discussed in greater depth in Section 5.5 of Yamamoto and Yoden (2013).

sufficiently so that $\mathcal{R} \gg 1$, S stops increasing with decreasing Ω, and instead saturates at a constant value $S \approx 1/2$. Over the entire parameter space considered, S in the 3D and axisymmetric experiments (S_{3D} and S_{ax}) are always of the same order of magnitude (Figure 4). Eddies are unable to substantially modify S_{3D} away from S_{ax}, and instead S_{3D} takes the form of perturbations about S_{ax}. At high rotation rate, eddies induce down-gradient transport of m which causes $S_{3D} < S_{ax}$, while at low rotation rate, eddies induce up-gradient transport of m which leads to $S_{3D} > S_{ax}$. At both *very high* and *very low* rotation rates S_{3D} and S_{ax} converge. In the high rotation rate limit, this is because the characteristic scale of eddies generated by baroclinic instability decreases as the rotation rate is increased. In the low rotation rate limit, we suggest that this is due to a collapse of the instability accelerating equatorial super-rotation when the rotation rate is decreased sufficiently, although a full investigation of this collapse is left for future work.

We are able to capture the dependence of S on Ω (or more generally $\mathcal{R}$) obtained in our numerical experiments with an axisymmetric theoretical model for S (Figure 6), that we derive from the model of Held and Hou (1980). In the rapid rotation rate limit ($\mathcal{R} \ll 1$), the theoretical model predicts $S \approx \mathcal{R}/2$, and in the low rotation rate limit ($\mathcal{R} \gg 1$), the theoretical model predicts that $S \approx 2/5$, both of which are consistent with the results of our numerical experiments. By considering the limiting behaviour of our theory, we showed how the value of S and its local dependence on $\mathcal{R}$ is related to the dominance of different dynamical balances in the atmosphere. $S \ll 1$ and $S \propto \mathcal{R}$ defines a regime where geostrophic thermal wind balance is dominant throughout the domain, and $S \approx 1/2 =$ constant defines a regime dominated by conservation of angular momentum within the overturning circulation. In this scenario, the dominant momentum balance is geostrophic at low latitudes, and cyclostrophic at middle and high latitudes.

By considering our axisymmetric theory in tandem with an alternative theory for S proposed by Yamamoto and Yoden (2013), which defines a cyclostrophic regime when $S \gg 1$ and $S \propto \sqrt{\mathcal{R}}$ or $S \propto \mathcal{R}^{1/3}$, we are able to characterise each of the circulation regimes accessed by our numerical experiments, and the Solar System planets (Figure 7). In particular, our analysis makes clear that the atmospheres of Venus and Titan, characterised by cyclostrophic balance and strong equatorial super-rotation, are in a fundamentally different dynamical regime to our Earth-like simulations in their low rotation rate limit. With this in mind, we argue that slowly rotating planets do not enter a cyclostrophic, strongly super-rotating regime by 'default', as is often assumed.

In the present study, we have demonstrated that the global super-rotation index S is a useful quantity to study when comparing the dynamics of different planetary atmospheres. We hope that this work, in combination with that of Yamamoto and Yoden (2013), will provide a framework for future work to make more use of S.

Acknowledgments. We would like to thank Mark Hammond for engaging in discussions which benefited this work, and Man-Suen Chan for IT support. We are grateful to all those who have contributed to the development of the `Isca` modelling framework (see `https://ex.ac.uk/isca`). The authors were supported by STFC grants ST/S505638/1, ST/S000461/1 and ST/N00082X/1.

Data availability statement. All model output data presented in this work will be made available upon reasonable request to the authors. The numerical code used in this work can be obtained from `https://github.com/ExeClim/Isca`.

APPENDIX A

Relation between S and S' for YY model

Yamamoto and Yoden (2013, YY) consider a non-dimensional measure of super-rotation strength S', defined as

$$S' \equiv \frac{U}{\Omega a}, \tag{A1}$$

where U is a scale for the zonal velocity at the model top. S', like S, is an internal Rossby number.

When deriving their theory for S', YY assume that the meridionally integrated 'relative' component of specific angular momentum $m_r = u \times a\cos\vartheta$,

$$m_0(z) = \int_0^{\frac{\pi}{2}} m_r(\vartheta, z)\cos\vartheta\, \mathrm{d}\vartheta, \tag{A2}$$

has the following vertical structure:

$$m_0(z) = Ua\left[1 - \cos\left(\frac{\pi z}{H}\right)\right]/2, \tag{A3}$$

where H is the height at the model top.

As YY specify a vertical structure for their model, we may relate S', which measures super-rotation at the model top, to the global super-rotation index S,

$$S = \frac{\frac{Ua}{2}\int_0^H \left[1 - \cos\left(\frac{\pi z}{H}\right)\right] \mathrm{d}z}{\Omega a^2 H \int_0^{\frac{\pi}{2}} \cos^3\vartheta\, \mathrm{d}\vartheta} = \frac{3}{4}S'. \tag{A4}$$

References

Andrews, D. G., J. D. Mahlman, and R. W. Sinclair, 1983: Eliassen-Palm Diagnostics of Wave-Mean Flow Interaction in the GFDL "SKYHI" General Circulation Model. *J. Atmos. Sci.*, **40**, 2768–2784, doi:10.1175/1520-0469(1983)040<2768:ETWATM>2.0.CO;2.

Bird, M. K., and Coauthors, 2005: The vertical profile of winds on Titan. *Nature*, **438**, 800–802, doi:10.1038/nature04060.

Boer, G. J., 1982: Diagnostic Equations in Isobaric Coordinates. *Mon. Weather Rev.*, **110 (12)**, 1801, doi:10.1175/1520-0493(1982)110<1801:DEIIC>2.0.CO;2.

Colyer, G. J., and G. K. Vallis, 2019: Zonal-Mean Atmospheric Dynamics of Slowly Rotating Terrestrial Planets. *J. Atmos. Sci.*, **76**, 1397–1418, doi:10.1175/JAS-D-18-0180.1.

Counselman, C. C., S. A. Gourevitch, R. W. King, G. B. Loriot, and E. S. Ginsberg, 1980: Zonal and meridional circulation of the lower atmosphere of Venus determined by radio interferometry. *J. Geophys. Res.*, **85**, 8026–8030, doi:10.1029/JA085iA13p08026.

Dias Pinto, J. R., and J. L. Mitchell, 2014: Atmospheric superrotation in an idealized GCM: Parameter dependence of the eddy response. *Icarus*, **238**, 93–109, doi:10.1016/j.icarus.2014.04.036.

Fang, M., and K. K. Tung, 1999: Time-Dependent Nonlinear Hadley Circulation. *J. Atmos. Sci.*, **56 (12)**, 1797–1807, doi:10.1175/1520-0469(1999)056<1797:TDNHC>2.0.CO;2.

Flasar, F. M., and R. K. Achterberg, 2009: The structure and dynamics of Titan's middle atmosphere. *Phil. Trans. Roy. Soc. London Ser. A*, **367**, 649–664, doi:10.1098/rsta.2008.0242.

Fulchignoni, M., and Coauthors, 2005: In situ measurements of the physical characteristics of Titan's environment. *Nature*, **438 (7069)**, 785–791, doi:10.1038/nature04314.

Geisler, J. E., E. J. Pitcher, and R. C. Malone, 1983: Rotating-Fluid experiments with an atmospheric general circulation model. *J. Geophys. Res.*, **88**, 9706–9716, doi:10.1029/JC088iC14p09706.

Gierasch, P. J., 1975: Meridional circulation and the maintenance of the Venus atmospheric rotation. *J. Atmos. Sci.*, **32**, 1038–1044, doi:10.1175/1520-0469(1975)032<1038:MCATMO>2.0.CO;2.

Held, I. M., 2018: 100 Years of Progress in Understanding the General Circulation of the Atmosphere. *Meteorological Monographs*, Vol. 59, 6.1–6.23, doi:10.1175/AMSMONOGRAPHS-D-18-0017.1.

Held, I. M., and A. Y. Hou, 1980: Nonlinear Axially Symmetric Circulations in a Nearly Inviscid Atmosphere. *J. Atmos. Sci.*, **37**, 515–533, doi:10.1175/1520-0469(1980)037<0515:NASCIA>2.0.CO;2.

Held, I. M., and M. J. Suarez, 1994: A Proposal for the Intercomparison of the Dynamical Cores of Atmospheric General Circulation Models. *Bullet. Am. Meteorol. Soc.*, **75 (10)**, 1825–1830, doi:10.1175/1520-0477(1994)075<1825:APFTIO>2.0.CO;2.

Hide, R., 1969: Dynamics of the Atmospheres of the Major Planets with an Appendix on the Viscous Boundary Layer at the Rigid Bounding Surface of an Electrically-Conducting Rotating Fluid in the Presence of a Magnetic Field. *J. Atmos. Sci.*, **26**, 841–853, doi:10.1175/1520-0469(1969)026<0841:DOTAOT>2.0.CO;2.

Hou, A. Y., 1984: Axisymmetric circulations forced by heat and momentum sources - A simple model applicable to the Venus atmosphere. *J. Atmos. Sci.*, **41**, 3437–3455, doi:10.1175/1520-0469(1984)041<3437:ACFBHA>2.0.CO;2.

Hourdin, F., O. Talagrand, R. Sadourny, R. Courtin, D. Gautier, and C. P. Mckay, 1995: Numerical simulation of the general circulation of the atmosphere of Titan. *Icarus*, **117 (2)**, 358–374, doi:10.1006/icar.1995.1162.

Kaspi, Y., and A. P. Showman, 2015: Atmospheric Dynamics of Terrestrial Exoplanets over a Wide Range of Orbital and Atmospheric Parameters. *Astrophys. J.*, **804**, 60, doi:10.1088/0004-637X/804/1/60.

Lebonnois, S., C. Covey, A. Grossman, H. Parish, G. Schubert, R. Walterscheid, P. Lauritzen, and C. Jablonowski, 2012: Angular momentum budget in General Circulation Models of superrotating atmospheres: A critical diagnostic. *Journal of Geophysical Research (Planets)*, **117 (E12)**, E12004, doi:10.1029/2012JE004223.

Lebonnois, S., F. Hourdin, V. Eymet, A. Crespin, R. Fournier, and F. Forget, 2010: Superrotation of Venus' atmosphere analyzed with a full general circulation model. *J. Geophys. Res. Planets*, **115**, E06006, doi:10.1029/2009JE003458.

Lebonnois, S., and Coauthors, 2013: Models of Venus Atmosphere. *Towards Understanding the Climate of Venus*, L. Bengtsson, R.-M. Bonnet, D. Grinspoon, S. Koumoutsaris, S. Lebonnois, and D. Titov, Eds., 129, doi:10.1007/978-1-4614-5064-1_8.

Lee, S., 2005: Baroclinic Multiple Zonal Jets on the Sphere. *J. Atmos. Sci.*, **62 (7)**, 2484–2498, doi:10.1175/JAS3481.1.

Lu, L. L., and M. Yamamoto, 2020: Planetary-size dependence of zonal jets: Effects of horizontal diffusion in an idealized Earth-like general circulation model. *Planet. Space Sci.*, **70**, 104 976, doi:doi.org/10.1016/j.pss.2020.104976.

Mendonça, J. M., and P. L. Read, 2016: Exploring the Venus global super-rotation using a comprehensive general circulation model. *Planet. Space Sci.*, **134**, 1–18, doi:10.1016/j.pss.2016.09.001.

Mitchell, J. L., and G. K. Vallis, 2010: The transition to superrotation in terrestrial atmospheres. *J. Geophys. Res. Planets*, **115**, E12008, doi:10.1029/2010JE003587.

Porco, C. C., and Coauthors, 2003: Cassini Imaging of Jupiter's Atmosphere, Satellites, and Rings. *Science*, **299 (5612)**, 1541–1547, doi:10.1126/science.1079462.

Porco, C. C., and Coauthors, 2005: Cassini Imaging Science: Initial Results on Saturn's Atmosphere. *Science*, **307 (5713)**, 1243–1247, doi:10.1126/science.1107691.

Potter, S. F., G. K. Vallis, and J. L. Mitchell, 2014: Spontaneous Super-rotation and the Role of Kelvin Waves in an Idealized Dry GCM. *J. Atmos. Sci.*, **71**, 596–614, doi:10.1175/JAS-D-13-0150.1.

Read, P. L., 1986a: Super-rotation and diffusion of axial angular momentum. I. "Speed limits" for axisymmetric flow in a rotating cylindrical fluid annulus. *Q. J. R. Meteorol. Soc.*, **112 (471)**, 231–251, doi:10.1002/qj.49711247113.

Read, P. L., 1986b: Super-rotation and diffusion of axial angular momentum. II. A review of quasi-axisymmetric models of planetary atmospheres. *Q. J. R. Meteorol. Soc.*, **112**, 253–272, doi:10.1002/qj.49711247114.

Read, P. L., 2011: Dynamics and circulation regimes of terrestrial planets. *Planet. Space Sci.*, **59**, 900–914, doi:10.1016/j.pss.2010.04.024.

Read, P. L., and S. Lebonnois, 2018: Superrotation on Venus, on Titan, and Elsewhere. *Ann. Rev. Earth Planet. Sci.*, **46**, 175–202, doi:10.1146/annurev-earth-082517-010137.

Read, P. L., S. R. Lewis, and G. K. Vallis, 2018: Atmospheric Dynamics of Terrestrial Planets. *Handbook of Exoplanets*, H. Deeg, and J. Belmonte, Eds., Springer, Cham.

Sánchez-Lavega, A., S. Lebonnois, T. Imamura, P. Read, and D. Luz, 2017: The Atmospheric Dynamics of Venus. *Space Sci. Rev.*, **212**, 1541–1616, doi:10.1007/s11214-017-0389-x.

Schneider, T., 2006: The General Circulation of the Atmosphere. *Ann. Rev. Earth Planet. Sci.*, **34**, 655–688, doi:10.1146/annurev.earth.34.031405.125144.

Schneider, T., and C. C. Walker, 2008: Scaling Laws and Regime Transitions of Macroturbulence in Dry Atmospheres. *J. Atmos. Sci.*, **65 (7)**, 2153, doi:10.1175/2007JAS2616.1.

Showman, A. P., R. D. Wordsworth, T. M. Merlis, and Y. Kaspi, 2013: Atmospheric Circulation of Terrestrial Exoplanets. *Comparative Climatology of Terrestrial Planets*, S. J. Mackwell, A. A. Simon-Miller, J. W. Harder, and M. A. Bullock, Eds., 277, doi:10.2458/azu_uapress_9780816530595-ch12.

Thompson, R. O. R. Y., 1980: A Prograde Jet Driven by Rossby Waves. *J. Atmos. Sci.*, **37 (6)**, 1216–1226, doi:10.1175/1520-0469(1980)037<1216:APJDBR>2.0.CO;2.

Vallis, G. K., and Coauthors, 2018: Isca, v1.0: a framework for the global modelling of the atmospheres of Earth and other planets at varying levels of complexity. *Geosci. Model Dev.*, **11**, 843–859, doi:10.5194/gmd-11-843-2018.

Wang, P., and J. L. Mitchell, 2014: Planetary ageostrophic instability leads to superrotation. *Geophys. Res. Lett.*, **41**, 4118–4126, doi:10.1002/2014GL060345.

Wang, Y., P. L. Read, F. Tabataba-Vakili, and R. M. B. Young, 2018: Comparative terrestrial atmospheric circulation regimes in simplified global circulation models. Part I: From cyclostrophic super-rotation to geostrophic turbulence. *Q. J. R. Meteorol. Soc.*, **144**, 2537–2557, doi:10.1002/qj.3350.

Williams, G. P., 1978: Planetary circulations. I. Barotropic representation of Jovian and terrestrial turbulence. *J. Atmos. Sci.*, **35**, 1399–1426, doi:10.1175/1520-0469(1978)035<1399:PCBROJ>2.0.CO;2.

Williams, G. P., 2003: Barotropic Instability and Equatorial Superrotation. *J. Atmos. Sci.*, **60**, 2136–2152, doi:10.1175/1520-0469(2003)060<2136:BIAES>2.0.CO;2.

Williams, G. P., 2006: Equatorial Superrotation and Barotropic Instability: Static Stability Variants. *J. Atmos. Sci.*, **63**, 1548–1557, doi:10.1175/JAS3711.1.

Yamamoto, H., K. Ishioka, and S. Yoden, 2009: Axisymmetric steady solutions in an idealized model of atmospheric general circulations: Hadley circulation and super-rotation. *Theor. and Appl. Mech. Japan*, **57**, 147–158, doi:10.11345/nctam.57.147.

Yamamoto, H., and S. Yoden, 2013: Theoretical estimation of the superrotation strength in an idealized quasi-axisymmetric model of planetary atmospheres. *J. Meteorol. Soc. Japan*, **91 (2)**, 119–141, doi:10.2151/jmsj.2013-203.